Journal of Catalysis **207,** 88–100 (2002)
doi:10.1006/jcat.2002.3532, available online at http://www.idealibrary.com on IDEAL®

Manganese Oxide–Silica Aerogels: Synthesis and Structural and Catalytic Properties in the Selective Oxidation of NH_3

P. Fabrizioli, T. Bürgi, and A. Baiker[1]

Laboratory of Technical Chemistry, Swiss Federal Institute of Technology, ETH, Hönggerberg-HCI, CH-8093 Zürich, Switzerland

Received October 16, 2001; revised January 4, 2002; accepted January 4, 2002

Manganese oxide–silica mixed oxide aerogels with different morphological and chemical properties were prepared using the sol–gel method and ensuing extraction of the solvent with supercritical CO_2. Two types of manganese precursor, varying hydrolysis conditions of the silica and manganese precursors, influence of base addition for gelation, and calcination temperatures were investigated. Base addition had a strong effect on textural properties, producing high-surface-area, mesoporous aerogels, whereas these properties were only marginally affected by kind of manganese precursor used. The presence of different manganese oxide species was evidenced by X-ray diffraction, Raman and diffuse reflectance infrared Fourier transform spectroscopy, and temperature-programmed reduction. Mn^{4+}, Mn^{3+}, and Mn^{2+} oxide species were found after calcination at 600°C in air. Sol–gel processing with manganese(II) nitrate resulted in highly dispersed mixed oxides. Basic gelation of these sols strongly influenced the state of the manganese, leading to crystallites of hausmannite and to amorphous Mn_5O_8 in the calcined samples. Aerogels derived from the less reactive Mn(III) $(acac)_3$ did not contain any manganese oxide crystallites when prepared under the same basic conditions. The catalytic performance of the aerogels in the selective oxidation of ammonia strongly depended on the state of the manganese. Samples containing crystalline Mn_3O_4 were more active than amorphous aerogels with dispersed manganese oxide species and afforded high selectivity to N_2O. The presence of amorphous Mn_5O_8 further increased the activity and the selectivity to nitrous oxide, reaching 74% at 360°C. Nitrogen formation was found to be related to the amount of strongly Lewis-bound ammonia. The amorphous aerogels showing more Lewis-bound ammonia produced mainly nitrogen below 480°C, affording a selectivity of 78% at 360°C. © 2002 Elsevier Science (USA)

Key Words: **manganese oxide–silica aerogels; selective oxidation of ammonia; supercritical drying; hausmannite; Mn_5O_8; Brønsted and Lewis acidity.**

1. INTRODUCTION

Aerogel catalysts (1–3) offer unique morphological and chemical properties, which originate from their wet-chemical preparation (solution–sol–gel method) and the subsequent removal of the solvent by supercritical drying. Extraction of the solvent using supercritical carbon dioxide is a particularly "gentle" drying method, as temperature can be kept as low as 40°C. Materials with large porosity and specific surface area are obtained, and control over the sol–gel conditions offers the possibility of preparing highly dispersed mixed oxides.

Here we report on the synthesis and structural properties of manganese oxide–silica low-temperature aerogels and their catalytic performance in the selective catalytic oxidation of ammonia.

A variety of manganese-containing catalyst materials has been reported in the past. Silica-supported manganese oxide catalysts were studied for application in CO oxidation (4) and oxidative coupling of methane (5). Various catalysts with low valent manganese oxides were applied for gas-phase reactions, such as CO hydrogenation (6), methane high-temperature combustion (7, 8), and, important in air pollution control, selective catalytic reduction of NO by hydrocarbons (9, 10) and by ammonia (11–13). Manganese grafted onto various oxides was studied by Ma *et al.* (14, 15). Sol–gel processing was reported for the syntheses of silica-supported spinel $LiMn_2O_4$ (16, 17), manganese oxide silica monolithic gels (18), $MnAl_2O_4$ (19), $(Mg_{(6-x)}Al_x)MnO_8$ (20), and octahedral molecular sieves (21), and for the preparation of porous manganese oxides for lithium insertion (22–24). Li–Mn–O aerogels were prepared by Passerini *et al.* (25) and Mn-substituted barium hexaaluminates aerogels by Yan and Thompson (26).

The selective catalytic oxidation (SCO) of ammonia to nitrogen is important in waste gas treatment, to eliminate effluent ammonia stemming from the ammonia used as reducing agent in the selective catalytic reduction of nitrogen oxides. Due to fluctuations in temperature and NO_x content, ammonia is used in excess and ammonia slip is inevitable under working conditions. Active catalysts in the temperature range 280–480°C are needed for ammonia oxidation. Further applications of SCO are the treatment of reformates for fuel-cell systems and the deodorization of ammonia-containing gas. In addition to the manganese oxides MnO_2 (27) and Mn_2O_3 (28), supported manganese

[1] To whom correspondence should be addressed. Fax: +41 1 632 11 63. E-mail: baiker@tech.chem.ethz.ch.

0021-9517/02 $35.00

oxide (29–31), SiO_2-pillared manganese titanate (32), perovskite oxides (33), Mn-hexaaluminate (34), and Mn–ZSM-5 (35) have been applied for SCO.

2. EXPERIMENTAL

2.1. Preparation of Aerogels

Different sol–gel conditions were applied for the synthesis of MnO_x–SiO_2 aerogels with a nominal content of 10 wt% Mn_2O_3, based on the theoretical system Mn_2O_3–SiO_2 (10 wt% Mn_2O_3 corresponds to 7 wt% Mn or 2.6 at% Mn). The conditions of the applied sol–gel routes are summarized in Table 1. In general, tetraethoxysilicon(IV) and manganese(II) nitrate or manganese(III) acetylacetonate were used as precursors. The hydrolysant was composed of nitric acid, water, and ethanol. Optionally, gel formation was induced by addition of a base. The sol–gel process was carried out at ambient temperature ($25 \pm 2^\circ$C) and under nitrogen atmosphere in a 250-ml glass flask wrapped up with aluminium foil in order to avoid photocatalytic oxidation of solvated Mn^{2+} (36). A magnetic bead of 2.5-cm length was used for stirring.

The aerogels were divided into three groups, depending on their structural properties and on the synthesis procedure used. For the sake of brevity a set of acronyms is used to distinguish the aerogels. The letters *a*, *b*, and *c*, followed arbitrarily by a numeral, denote the following: *a*, aerogels prepared with manganese nitrate without base addition; *b*, aerogels prepared with manganese nitrate and forced gelation using a nitrogen-containing base; and *c*, aerogels derived from $Mn(acac)_3$ as manganese precursor.

In the following the general synthesis route for the samples prepared with manganese nitrate as precursor is described. Some 46.23 g of tetraethoxysilicon(IV) (TEOS; Fluka, puriss.) was dissolved in 60 ml of ethanol (EtOH; Fluka, puriss.) and homogenized under nitrogen. The hydrolysant was prepared from nitric acid (HNO_3; 65%, Merck, p.a.) and doubly distilled water. Then 4.71 g of manganese(II) nitrate ($Mn(NO_3)_2 \cdot 4H_2O$; Fluka, purum, >97%) was completely dissolved in 15.98 g of hydrolysant with a pH of 2.5; the solution was then diluted with 15 ml of ethanol and added under vigorous stirring (600 rpm) to the TEOS solution. A clear and slightly pink sol was obtained. After 65 h a clear, pink, viscous gel (*a1*) was formed, which was allowed to age for 25 h. Prehydrolysis of the tetraethoxysilicon was applied for sample *a2*. The acid hydrolysant was added directly to the dissolved TEOS and the sol was refluxed at 60°C for 1.5 h under stirring. The manganese(II) nitrate tetrahydrate was dissolved in 15 ml of EtOH under water- and oxygen-free conditions inside a glove box and added to the prehydrolyzed TEOS solution. A noticeable increase in viscosity was observed after 120 h, and the viscous gel was allowed to age for 25 h.

Sample *b1* was synthesized analogously to *a1*; however, 14 h after preparation of the sol under vigorous stirring, gelation was forced by ammonium hydroxide (NH_4OH; Fluka, puriss. p.a., 25 wt% in water) diluted in EtOH ($V_{NH_4OH(aq)} : V_{EtOH} = 1:6$). Then 12 ml of the basic solution was added in drops (1 ml/min) and a bright-to-dark-brown gel was obtained 2 min after. A pure silica gel (*Sib1*) was prepared analogously to *b1*. The sol gelled after introducing 3.5 ml of the basic ammonia solution.

TABLE 1

Conditions Applied for Sol–Gel Syntheses of MnO_x/SiO_2 Aerogels

Aerogel[a]	H_2O[b] : TEOS : HNO_3 : EtOH (molar ratio)	Gelation agent	Base : TEOS (molar ratio)	EtOH added (ml)	Hydr. time[c] (h)	Gel time[d] (h)
a1	4.34 : 1 : 0.00023 : 5.7	—	—	—	—	65
a2[e]	4.34 : 1 : 0.00023 : 5.7	—	—	—	—	120
b1	4.34 : 1 : 0.00023 : 5.7	NH_4OH	0.050 : 1	10	14	0.23
b2	4.34 : 1 : 0.00023 : 5.7	*N,N*-d.a.[f]	0.085 : 1	9	14	0.70
b3	4.34 : 1 : 0.00023 : 5.7	*N,N*-d.a.[f] + NH_4OH	0.230 : 1	59	14	0.70
b4	2.34 : 1 : 0.01 : 5.7	NH_4OH	0.100 : 1	20	14	1.57
Si*b1*	4 : 1 : 0.00023 : 5.7	NH_4OH	0.013 : 1	20	14	0.06
c1	2 : 1 : 0.01 : 5.7[g]	NH_4OH	0.100 : 1	20	14	72

[a] Acronyms of aerogels are explained in Section 2.1.

[b] In the case where $Mn(NO_3)_2 \cdot 4H_2O$ was used, additional water to that of the acid hydrolysant was introduced, corresponding to H_2O_{salt} : TEOS = 0.34 : 1.

[c] Hydrolysis time, i.e., from the addition of the hydrolysant to the addition of the basic solution.

[d] For the samples with forced gelation, the time from the beginning of the base addition to gel formation is reported, whereas for gels *a1* and *a2*, the time from the addition of the hydrolysant to gel formation is noted. Gels without base addition, as well as the slowly gelled *c1*, were allowed to age for 25 h, whereas the other gels were immediately transferred to the autoclave.

[e] Prehydrolysis of TEOS was performed before addition of the manganese precursor.

[f] *N,N*-diethylaniline.

[g] The solvent for the samples prepared with $Mn(acac)_3$ was composed of acetylacetone (20 vol%) and EtOH (80 vol%).

Sol *b4* was prepared by using 8.20 g of hydrolysant with a pH of 0.5. Some 24 ml of an ammonia solution ($V_{NH_4OH(aq)} : V_{EtOH} = 1:6$) was added in drops (1 ml/min): 12 ml was added, and after 30 min another 12 ml. Forty minutes later a brown, but clear, stiff gel formed.

Two gels were prepared by addition of *N,N*-diethylaniline: 14 h after preparation of the sol, gelation was induced by adding 12 ml of an alcoholic *N,N*-diethylaniline solution ($V_{N,N\text{-diethylaniline}} : V_{EtOH} = 1:3$). After 30 min the viscosity significantly increased. The slightly brown gel (*b2*) was aged for 90 min. For gel *b3*, after addition of *N,N*-diethylaniline, 55 ml of a $NH_4OH_{(aq)}$–EtOH solution ($V_{NH_4OH(aq)} : V_{EtOH} = 1:10$) was added to the viscous sol and a brown gel formed.

In general, addition of aqueous ammonia ($pK_a = 9.25$) to the sol led to change in the color from pale pink to dark brown. For sample *b1* light and dark brown areas could be discerned. The weaker base *N,N*-diethylaniline ($pK_a = 6.6$) (37) led only to a slight darkening of the sol.

The sample prepared with $Mn(acac)_3$ was hydrolyzed by a nitric acid–water solution with pH 0.5, as acid conditions favor the decomposition of the complex necessary for the incorporation of the manganese into the silica matrix. In general, 6.60 g of $Mn(acac)_3$ (Riedel de Haen, purum) was solved in 30 ml of an ethanol–acetylacetone solution (1 : 1) (both Fluka, puriss. p.a.) by heating it briefly to 60°C. TEOS (46.23 g) was dissolved in 40 ml of EtOH. Then 8.20 g of the hydrolysant was added to the $Mn(acac)_3$ solution. The solution was stirred for 15 min and then added to the dissolved TEOS. After 14 h, 12 ml of a basic solution ($V_{NH_4OH(aq)} : V_{EtOH} = 1:6$) was added to the sol over the course of 12 min, and 12 ml again after 30 min. Three days later a brownish and highly viscous gel was formed, which was aged for 1 day (*c1*).

Supercritical drying. The gels prepared without base addition as well as the slowly gelled *c1* were aged for 1 day prior to extraction with supercritical CO_2, whereas the other, stiff gels were directly transferred into a 2-dm^3 autoclave and covered with 90 ml of EtOH. Within 1 h and at a temperature of 40°C, the autoclave was pressurized with CO_2 to 22 MPa and the liquid–gas separator to 1 MPa, which required 2.1 kg of CO_2. The solvent was semicontinuously extracted for 6 h using a CO_2 flow of 20 g min^{-1}. Finally, the CO_2 was isothermally released at a rate of ca. 20 g min^{-1}. The extracted powders were white in color for the samples without base addition. Those prepared with base addition were light brown or grey.

Calcination procedure. The raw aerogel powder (3 g) was calcined in a tubular reactor with upward flow. The reported temperature corresponds to the oven temperature. To remove part of the organic residues prior to calcination, all aerogel samples were heated in a nitrogen flow of 0.5 dm^3 min^{-1} at a rate of 5°C min^{-1} to 400°C and held at this temperature for 1 h. After cooling to ca. 80°C, they were heated at 5°C min^{-1} in air flowing at 0.5 dm^3 min^{-1} to 400 or 600°C and held for 5 h. A portion of *a1* was calcined at 950°C for 1 h. After calcination all samples were dark brown.

2.2. Physicochemical Characterization

Atomic absorption spectroscopy (AAS). To determine the manganese content 80 mg of dry catalyst was dissolved in 400 μl of hydrofluoric acid (HF; 40% in water, Fluka, 99.5%). The superfluous fluoride ions were neutralized with boric acid. In order to obtain stable solutions 2 g of 65% HNO_3 (Fluka, puriss.) was added before the solution was diluted to 50 ppm Mn. The catalyst solutions were analyzed on a VARIAN SpektrAA-10 atomic absorption spectrometer by comparison with standard solutions containing the same amount of silica (silica aerogel), fluoride ions, and boric and nitric acid as the catalyst solutions. Manganese was added from a manganese standard solution (Merck, Titrisol for standard solution).

C, H, N analysis. Total carbon, hydrogen, and nitrogen contents of the samples after calcination at 400 and 600°C were determined using a LECO CHN-900 elemental microanalysis apparatus.

Nitrogen physisorption. Prior to measurement, the samples were degassed to 0.1 Pa at 80°C. Textural properties were determined by nitrogen physisorption at −196°C using a Micromeritics ASAP 2000 instrument. The specific surface area (S_{BET}) was calculated in a relative pressure range of 0.01–0.20, assuming a cross-sectional area of 0.162 nm^2 for the nitrogen molecule. The estimated *C*-values were in the range 120–200. The specific desorption pore volume was assessed by the Barrett–Joyner–Halenda (BJH) method, which is assumed to cover the cumulative adsorption pore volume of pores with a maximum diameter in the range 1.7–300 nm. The assessment of microporosity was made from the *t*-plots ($0.4 < t < 0.6$), using the Harkins–Jura correlation.

X-ray diffraction (XRD). XRD measurements were performed on a Siemens D5000 powder X-ray diffractometer. The diffractograms were recorded using CuK_α radiation (2Θ range 15–65°) and a position-sensitive detector with Ni filter.

IR spectroscopy. IR spectra of the $Mn(acac)_3$ solutions were recorded on a Perkin Elmer System 2000 Fourier transform IR (FTIR) spectrometer at 4-cm^{-1} resolution. CaF_2 windows were used and spectra were measured at ambient condition.

Temperature-programmed reduction (TPR). The apparatus used for TPR measurements has been described elsewhere (38). The measurements were carried out using 5% hydrogen in argon as reductant and a flow rate of 75 ml min^{-1}. For each analysis the sample, which contained 0.4 mmol of Mn, taking into consideration the manganese content determined by AAS, was pretreated in air at 550°C

for 30 min. The temperature during reduction was ramped from 25 to 550°C at a rate of 5°C min^{-1}.

X-ray photoelectron spectroscopy (XPS). XPS analysis was performed using a Leybold LHS 11 instrument. MgK_α radiation (240 W) was applied to excite photoelectrons, which were detected with the analyzer operated at a 31-eV constant pass energy, resulting in a line width of 0.9 eV (full width at half-maximum) for the Ag $3d_{5/2}$ line. The energy scale of the spectrometer was calibrated versus the Au $4f_{7/2}$, Ag $3d_{5/2}$, and Cu $2p_{3/2}$ lines at 84.2, 367.9, and 932.4 eV. Correction of the energy shift, due to steady-state charging, was accomplished by taking the C 1s line from adsorbed hydrocarbons at 285.0 eV as an internal standard. Empirically derived atomic sensitivity factors were used for quantification (39).

Raman spectroscopy. Samples were diluted 5 wt% in KBr and pressed into a sample holder with an opening of 4-mm diameter. Spectra were excited using the 1064-nm line of a NdYAG laser (Spectron Laser Systems). The backscattered light was analyzed using a Perkin Elmer System 2000 instrument. A laser power of 600 mW was used and 4000 scans were accumulated with a resolution of 4 cm^{-1}.

Diffuse reflectance infrared Fourier transform spectroscopy (DRIFTS). DRIFT spectra were recorded on a Perkin Elmer System 2000 FTIR instrument with a diffuse reflectance cell and a controlled environmental chamber (both Spectra-Tech) equipped with CaF_2 windows. The sample was mounted on a heatable ceramic frit (Al_2O_3). Before measurements the catalyst was heated to 300°C for 1 h in a synthetic air stream (Pangas; 20% O_2 purity, 99.5%; 80% N_2 purity, 99.995%) and dried using a cooling trap with an isopropanol–dry ice mixture. Spectra were taken by accumulating 50 scans at a resolution of 4 cm^{-1}. Ammonia (3600 ppm in argon, ±2% relative certified, Carbagas, dried over a KOH-containing cartridge) was adsorbed at 50°C. Thereafter the cell was flushed with argon for 2.5 h. Temperature-programmed desorption of ammonia (NH_3-TPD) was performed at a rate of 5°C min^{-1}; spectra were taken by accumulating 50 scans at a resolution of 4 cm^{-1} every 50°C. The spectra in the reflection mode were transformed to the Kubelka–Munk function. Then they were normalized to the silica overtone vibration at 1848 cm^{-1} (combination mode of Si–O vibrations), as proposed by Vansant (40). In order to visualize the species resulting from NH_3 adsorption, the spectrum of the unloaded catalyst was subtracted.

2.3. Catalytic Tests

Catalytic tests for selective catalytic oxidation (SCO) of NH_3 were carried out in a continuous-flow fixed-bed microreactor made of a quartz glass tube with a 4-mm inner diameter. Volumes of 0.126 cm^3 corresponding to 45–90 mg of catalyst (particle size, 150–300 μm) were used for the measurements. The reaction gas mixture consisted of 2000 ppm NH_3 and 2.0% O_2 in a helium balance. The gas mixture was made from single-component gases in a helium (99.999%) balance (3600 ppm NH_3/He, 7% O_2/He certified, ±2%, Carbagas). Feed and product concentrations of NH_3, N_2, NO, N_2O, and O_2 were quantitatively analyzed online using a Balzers quadrupole mass spectrometer QMA 112A.

Conversion measurements as a function of temperature up to 480°C were carried out twice at a gas hourly space velocity of 24,000 h^{-1} (273 K, 1 atm; STP) after pretreatment of the catalysts in synthetic air (Pangas; 20% O_2 purity, 99.5%; 80% N_2 purity, 99.995%; 50 ml min^{-1}) at 550°C for 30 min. The pressure drop over the catalyst bed was below 0.13 bar at room temperature. For differential activity measurements the space velocity was gradually raised from 17,000 h^{-1} to 50,000 h^{-1} (STP), and the temperature was adjusted to keep the ammonia conversion below 20%, in order to approximate differential reactor conditions. Turnover frequency (TOF) calculations were referred to the bulk manganese content. For every measurement a balance over all nitrogen-containing compounds was calculated. Even for high conversions of ammonia, the deviation in the balance did not exceed ±3%, indicating that all species, consumed or formed, were accounted for.

3. RESULTS

The main variables changed in the sol–gel synthesis were type of manganese precursor, the optional prehydrolysis of the manganese and/or silica precursor, acidity of the sol, and type and amount of N-base used as gelation agent (see Table 1).

3.1. Textural and Structural Properties

Table 2 lists the textural properties of all aerogels. In general, the aerogels showed a type-IV isotherm with a type-H1 adsorption–desorption hysteresis according to IUPAC classification. As a representative example, Fig. 1 depicts the adsorption–desorption isotherms and the pore size distribution of aerogels *a1* and *b1* calcined at 600°C. Base addition with forced gelation led to more-prominent mesoporosity, narrower pore size distribution, and higher surface area.

After calcination at 600°C, the BET surface area of the aerogels was in the range 390–770 m^2 g^{-1}, with the aerogels with forced basic gelation showing generally higher surface areas. The pore volumes were in the range 0.7–1.7 cm^3 g^{-1}, except for *b3*, which showed 2.2 cm^3 g^{-1}. The aerogels prepared from manganese nitrate with forced basic gelation had narrow pore size distribution, with maxima in the range 13–25 nm. Increasing the acidity of the sol in sample *b4* led to slightly higher surface area and mesoporosity in comparison to *b1*. The sample with the highest surface area and mesoporosity of all aerogels, *b3*, showed a BET surface area of 773 m^2 g^{-1} and a pore volume of

TABLE 2

Textural Properties of Manganese Oxide–Silica Aerogels

Aerogel[a]	Calcination temperature (°C)	S_{BET} ($m^2\ g^{-1}$)	S_{MP}[b] ($m^2\ g^{-1}$)	V_P[c] ($cm^3\ g^{-1}$)	dv_{max}[d] (nm)
a1	400	405	225	0.67	60
	600	387	191	0.74	50
	950	82	0	0.51	40
a2	600	436	199	0.95	38
b1	600	553	108	1.00	18
b2	600	513	187	0.87	13
b3	600	773	80	2.24	25
b4	600	663	100	1.60	22
c1	600	690	138	1.67	n.d

[a] Acronyms of aerogels are explained in Section 2.1.

[b] S_{MP} denotes the specific micropore surface area derived from *t*-plot analysis; corresponding specific micropore volumes ranged from 0 to 0.1 $cm^3\ g^{-1}$.

[c] V_P designates the BJH cumulative desorption pore volume of pores with maximum diameters in range 1.7–300 nm.

[d] dv_{max} is the graphically assessed pore size maximum of the pore size distribution derived from the adsorption branch.

2.24 $cm^3\ g^{-1}$, and the maximum pore size distribution was 25 nm. The aerogels without base addition (*a1*, *a2*) showed a noticeable share of micropores. The pore volumes were in the range 0.6–0.95 $cm^3\ g^{-1}$ and the maximum pore size distribution was 40–60 nm. The aerogel synthesized with $Mn(acac)_3$ and base addition *c1* had a very broad pore size distribution, and also macropores were found. Prehydrolysis of the TEOS for sample *a2* led to a narrower size distribution of the mesopores, whereas BET surface area and micropore share were nearly the same, as compared with the sample prepared without prehydrolysis. Calcination at 400°C was investigated for samples *a1*. Increasing the calcination temperature from 400 to 600°C resulted in a decrease in BET surface area and pore volume, mainly at the expense of micropores. Aerogel *a1*, calcined at 950°C, showed a five times lower surface area (82 $m^2\ g^{-1}$) than the same sample calcined at 600°C.

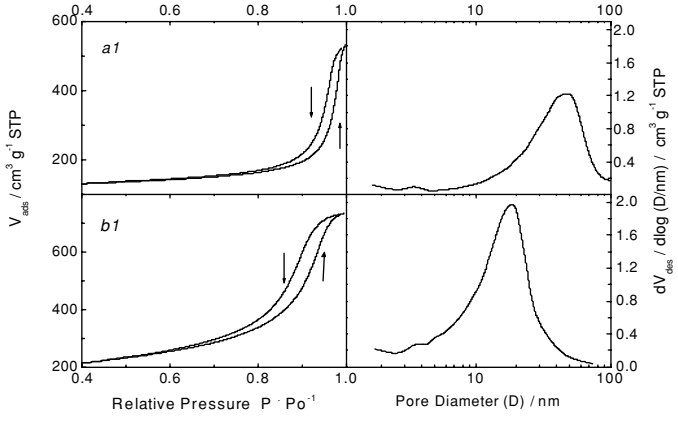

FIG. 1. Adsorption–desorption isotherm (left) and pore size distribution (right) of aerogels *a1* and *b1* calcined at 600°C.

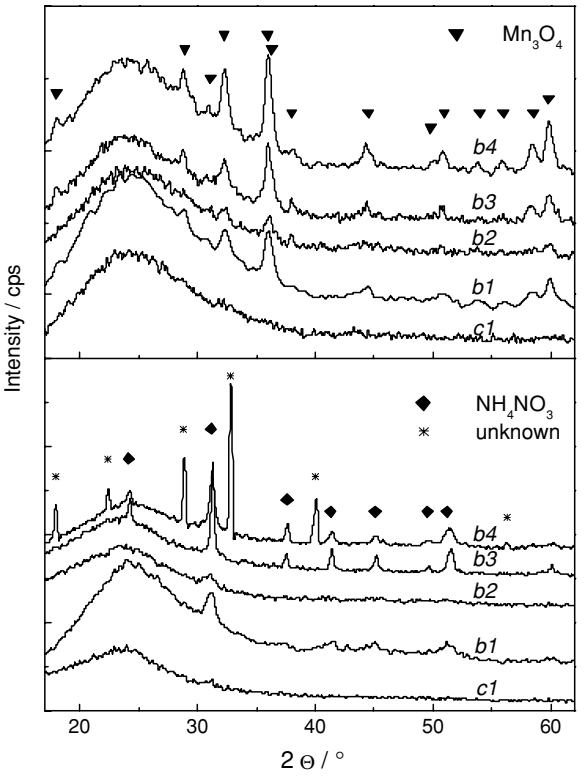

FIG. 2. XRD patterns of uncalcined aerogels *c1*, *b1*, *b2*, *b3*, and *b4* (bottom) and of the same aerogels calcined at 600°C in air (top). Sample *c1* and all other aerogels (not shown) were amorphous.

X-ray diffraction analysis of samples *b4*, *b3*, and *b1* calcined at 600°C showed reflections due to Mn_3O_4 crystallites (hausmannite), about 11–14 nm in size, as determined from the line broadening using the Scherrer equation (41) (Fig. 2, top). Note that tetragonal, metastable γ-Mn_2O_3 shows the same reflections; however, the presence of Mn_3O_4 was confirmed by Raman spectroscopy. Diffraction patterns corresponding to smaller crystallites were observed for sample *b2*. All samples gelled without base addition were X-ray amorphous, as was the sample produced from $Mn(acac)_3$, even though ammonia solution was used for gelation. In Fig. 2 (bottom) XRD patterns of some uncalcined aerogels are shown. A strong reflection at 31.3° together with less intense ones at 24.2, 37.7, 41.4, 45.1, 49.6, and 51.5° were present with samples that showed reflections due to hausmannite after calcination at 600°C. Their identity could not be determined. For the great variety of possible Mn(III) and (II, III) hydroxides and Mn(II, III) and (III, IV) oxide hydrates formed by oxidation of alkaline Mn(II) solutions, the reader is referred to Ref. (36). Acid aqueous solutions of Mn(II) nitrate were reported to contain predominantly the pink $Mn^{2+}(H_2O)_6$, as complete dissociation of the nitrate occurs. The hydrolysis of the hexaaquacomplex is low

at pH <7. In 1 M $Mn^{2+}{}_{(aq)}$ solutions with pH <4 no hydrolysis product was formed (42). In basic medium $Mn(OH)_2$ precipitates, which is partially redissolved in excess ammonia, probably due to complexation (43). Oxidation of the solvated Mn^{2+} is inhibited at low pH, whereas it proceeds fast in the presence of oxygen at high pH. Solvated Mn(III) is known to easily disproportionate in aqueous solution. We therefore suppose that oxidation of the manganese occurs, at least partially, during gelation in the case of basic conditions.

On the uncalcined *b4*, nitrammite (NH_4NO_3), originating from the sol–gel process, was detected. *a1* heated in air to 950°C showed formation of small α-Mn_2O_3 crystallites (not presented), although pure Mn_2O_3 was reported to transform to Mn_3O_4 in air at 870°C (36, 44).

Raman spectroscopy confirmed the presence of hausmannite on samples *b3*, *b4*, *b1*, and *b2*, by an intense vibration at 653–58 cm^{-1} (45, 46). The spectra of all calcined samples are shown in Fig. 3. The broad vibrations at 610, 800, 980, and 1100 cm^{-1} are due to amorphous silica (47). The bands at 650, 620, 530, and 585 cm^{-1} of sample *b3* are probably due to Mn_5O_8, whose vibrations were reported at 648, 617, 577, and 533 cm^{-1}. The spinel is composed of $Mn_2^{2+}Mn_3^{4+}O_8$ and could be isolated as an intermediate

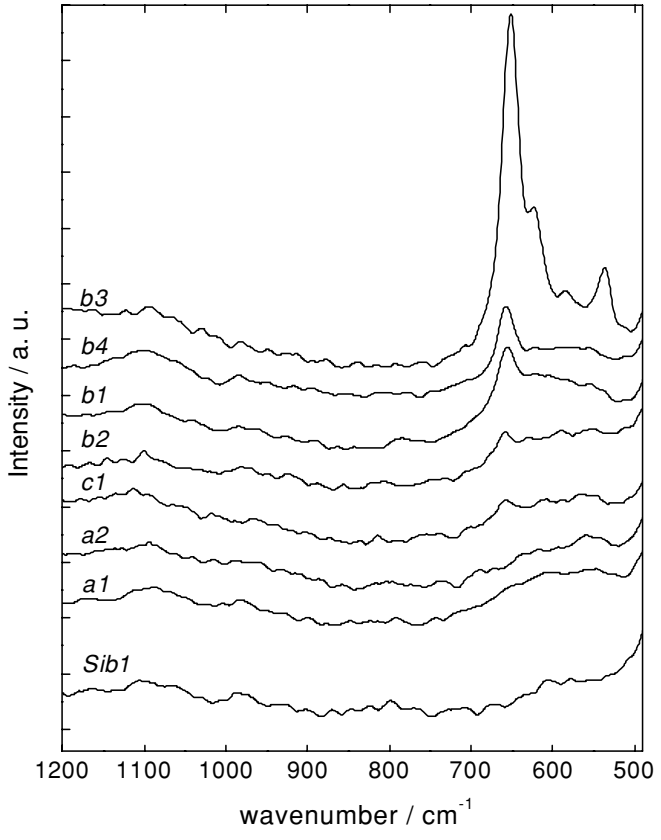

FIG. 3. RAMAN spectra of the calcined manganese oxide–silica aerogels; for comparison the spectra of the pure silica aerogel *Sib1* is shown.

TABLE 3

Manganese Content (AAS), Binding Energy for Mn $2p_{3/2}$, and Surface Composition (XPS), Surface-to-Bulk Manganese Ratio, and Mean Oxidation State (TPR) for Manganese Oxide–Silica Aerogels[a]

Aerogel	Mn(b) content (wt%)	Mn $2p_{3/2}$ (eV)	Mn(s)/Si(s) (at%/at%)	Mn(s)/Mn(b) (at%/at%)	Mean oxidation state (—)
a1	6.3	642.5	0.042	55	2.7
a2	6.0	642.6	0.032	47	2.8
b1	6.7	642.2	0.034	42	2.7
b2	6.1	642.2	0.043	61	2.6
b3	6.9	641.9	0.020	26	2.9
b4	6.7	642.4	0.054	67	2.9
c1	6.0	642.6	0.047	69	2.7
Mn_3O_4	—	640.6			2.7
Mn_2O_3	—	—			3.0

[a] (b) and (s) refer to bulk and surface, respectively.

during the oxidation of high-surface-area Mn_3O_4 to Mn_2O_3 (48). The presence of Mn_5O_8 could not be confirmed by XRD, due to low crystallinity of this phase. On aerogel *c1*, a weak band at 655 cm^{-1} indicates the presence of manganese oxide not detectable by XRD. On uncalcined *b4* no vibration due to manganese oxide was detected.

3.2. Chemical Properties

Chemical properties were investigated using atomic absorption spectroscopy (AAS), X-ray photoelectron spectroscopy (XPS), temperature-programmed reduction (TPR), and DRIFT spectroscopy.

Composition. The manganese content, determined by AAS, varied among the aerogels and was in the range 6.0–6.9 wt% Mn, which is lower than the nominal content of 7.0 wt%. Some manganese was probably extracted with the solvent by the supercritical CO_2. After calcination in air at 600°C, the aerogels showed negligible amounts of carbon and nitrogen (0.1–0.3 wt%). The water content of the materials exposed to ambient conditions amounted to 8–12 wt%. Elemental composition of the surface region was investigated using XPS. The surface contents of manganese are listed in Table 3 together with the binding energy of the Mn $2p_{3/2}$ photoelectron measured for the calcined samples. Binding energies between 641.9 and 642.6 eV were found. The values were higher than the binding energies for bulk Mn_3O_4 (Riedel de Haen, purum), which amounted to 640.6 eV. This may indicate a strong interaction between manganese and silica, similar to that found for "surface manganese oxide" on alumina (46). The Mn $2p_{3/2}$ binding energy for Mn^{2+} in the spinel $MnSiO_3$ was reported to be 642.3 eV, compared to 641.4 eV for Mn_3O_4 (49). Nitrogen and carbon were only found in traces, in accordance with elemental analysis.

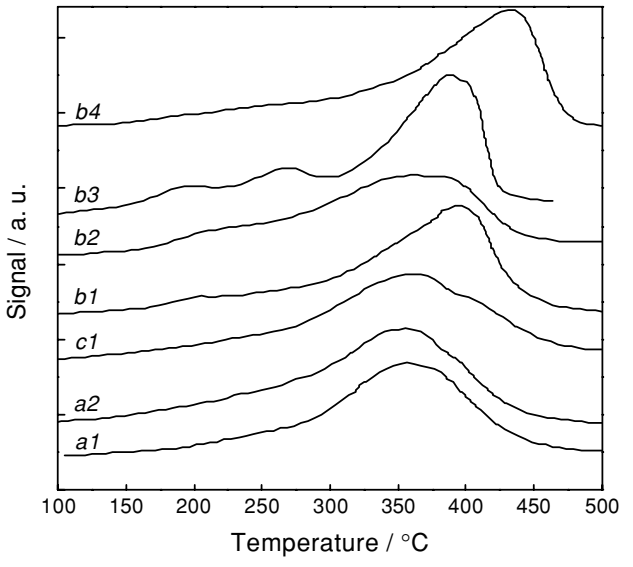

FIG. 4. Hydrogen consumption during temperature-programmed reduction of the aerogels calcined at 600°C.

In addition to the bulk manganese content, also the surface Mn/Si ratio varied with the sol–gel method applied (Table 3). For all aerogels enrichment of the manganese in the bulk and of silicon on the surface was found. For the aerogels prepared without base addition the ratio of surface-to-bulk manganese content, listed in Table 3, was 47–56%, and the bulk manganese content amounted to 6.0–6.3 wt%. Prehydrolysis of the TEOS afforded a lowering of the surface Mn content. The sample prepared by manganese nitrate and ammonia solution *b1* had a slightly lower surface-to-bulk ratio (42%) and a bulk content of 6.7 wt%. With increased acid content and ammonia addition (*b4*) a much higher surface-to-bulk ratio was found (67%). Gelation with *N,N*-diethylaniline (*b2*) resulted in a surface-to-bulk manganese ratio of 61% and 6.1 wt% bulk manganese. By adding ammonia solution to the same sol as prepared for *b2*, however, only 26% of the bulk manganese was detectable by XPS (*b3*). The bulk manganese content of this sample was maximal among all aerogels and amounted to 6.9 wt%. The sample prepared by manganese triacetylacetonate showed a bulk content of 6.0 wt% and a surface-to-bulk ratio of 69%.

Temperature-programmed reduction. TPR signals of the calcined aerogels are shown in Fig. 4. The reduction onset was at about 150°C for all samples, whereas for pure Mn_3O_4 the onset was at 400°C. Mn_3O_4 and Mn_2O_3 showed maximum hydrogen consumption during reduction to MnO at 483 and 478°C, respectively. Reduction of Mn_2O_3 to Mn_3O_4 occurs in the range 300–400°C (6). For the mixed oxide aerogels the maximum hydrogen consumption occurred between 350 and 430°C and hence at a much lower temperature than for the reference oxides. Reduction to Mn^{2+} was complete below 480°C for all aerogels.

All amorphous samples showed the maximum hydrogen consumption at 350–360°C. Further a shoulder at 380–400°C and a broadening of the signal toward lower temperature was observed, which was more pronounced with the samples prepared with manganese acetylacetonate, indicating greater heterogeneity of the manganese species. The mean oxidation state of these samples before reduction was calculated from the hydrogen consumption and amounted to 2.6–2.8 (Table 3).

The samples with crystalline Mn_3O_4 and Mn_5O_8 (*b1*, *b2*, *b3*, *b4*) showed maximum hydrogen consumption at a higher temperature than for the amorphous samples. The maximum was between 370 and 433°C and increased in the series $b2 < b3 \cong b1 < b4$. All samples, except *b4*, showed also some small signals in the range 170–270°C. The mean oxidation state was 2.9 for *b4* and *b3*, and 2.6–2.8 for the other samples (Table 3). The multiple step reduction in *b3* with weak peaks at 190 and 270°C may be explained by the presence of Mn^{4+} (Mn_5O_8), observed by Raman spectroscopy.

3.3. DRIFTS Studies

Hydroxyl groups. Figure 5 shows the DRIFT spectra of the aerogels after *in situ* pretreatment at 300°C in air.

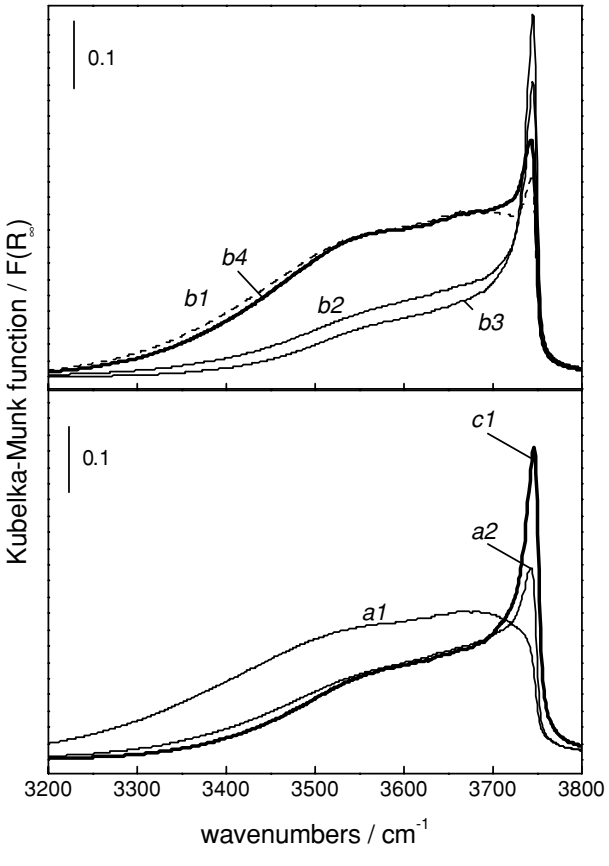

FIG. 5. DRIFT spectra of the calcined aerogels, dried *in situ* in air at 300°C. Top: Spectra of the aerogels with crystalline Mn_3O_4. Bottom: Spectra of the amorphous aerogels.

Among the samples with crystalline Mn_3O_4 (Fig. 5, top) the number of hydroxyl groups in the region 3700–3400 cm^{-1} decreased in the series *b4* ≅ *b1* > *b2* > *b3*. These hydroxyl groups are at least partly due to acid hydroxyl groups and may be assigned to Mn–OH–Si bridging hydroxyls, analogously to the bridging hydroxyls found at 3630–3660 cm^{-1} in aluminosilicates and ferrisilicates and to the hydroxyls in iron oxide–silica aerogels (50). For the amorphous samples (Fig. 5, bottom) the intensity of the vibrations decreased in the order *a1* > *c1* ≅ *a2*.

Ammonia adsorption. Ammonia adsorption at 50°C, after dehydration of the samples at 300°C, resulted in strong ν(NH) vibrations in the region 3400–2400 cm^{-1} (Fig. 6). No vibrations from the bulk catalyst interfere in this region. The total amount of adsorbed ammonia at 50 and 300°C is listed in Table 4.

Among the crystalline samples (Fig. 6, top) the amount of ammonia adsorbed at 50°C decreased in the order *b1* > *b4* ≅ *b2* > *b3*. *b1* showed broad bands in the range 2600–3100 cm^{-1} due to Brønsted-bound ammonia, whereas on the other samples the absorptions at 3368–3382 and 3281–3285 cm^{-1}, assigned to ν_{as}(N–H) and ν_s(N–H) of Lewis-bound ammonia, were dominant. During TPD the N–H stretching vibrations shifted to lower wavenumbers, indicating the presence of sites with different acidity on the catalyst. Strongly bound ammonia at 300°C was associated with bands at 3357–3373 and 3278–3282 cm^{-1}. The vibration at 3180 cm^{-1} was assigned to the overtone of the δ_{as}(NH) of the stronger bound Lewis species, in Fermi resonance with the nearby stretching vibration ν_s(NH), whereas the band at 3210 cm^{-1} was attributed to the overtone vibration of the weakly bound Lewis species (51), which is supported by the fact that at 300°C the latter band had almost completely vanished.

On the amorphous aerogels the stretching vibrations of Lewis-bound ammonia at 3361–74 (ν_{as}(NH)) and 3280–84 cm^{-1} (ν_s(NH)) were observed at lower wavenumbers than that on the crystalline samples (Fig. 6, bottom). *a1* showed intense bands due to Brønsted-bound ammonia at about 2800 and 3050 cm^{-1}; less intense bands were found on *a2*. After heating to 300°C these bands nearly disappeared and strongly Lewis-bound ammonia was detected at 3354–3362 and 3279–3280 cm^{-1}. The ammonia adsorption capacity at 50°C decreased in the order *a1* > *a2* > *c1* and was generally higher than for the samples with crystalline Mn_3O_4 (Table 4). Prehydrolysis of the silicon precursor afforded lower formation of acid sites with the aerogel prepared with manganese nitrate. For comparison the silica aerogel was investigated. The ammonium ions observed in the presence of gaseous ammonia immediately desorbed in argon atmosphere.

The broad band at 3200–3000 cm^{-1} is mainly composed of the symmetric and antisymmetric stretching vibrations of adsorbed NH_4^+. A combination band of the symmetric and antisymmetric deformation vibration of NH_4^+ species

TABLE 4

Ammonia Adsorption Uptakes at 50°C (N_{50}) and 300°C (N_{300}) Determined by DRIFTS

Aerogel	N_{50} (—)	N_{300} (—)	N_{300}/N_{50} (%)
a1	43	2.0	4.6
a2	20	0.5	2.5
b1	19	0.5	2.6
b2	14	0.8	5.7
b3	2	0.06	3.0
b4	15	0.3	2.0
c1	11	0.4	3.6

Note. The integrated intensities of the stretching vibrations in the 3400- to 3000-cm^{-1} region were used as a measure for the ammonia uptake. The ratio N_{300}/N_{50} is taken as a measure of the mean acidity of the catalysts.

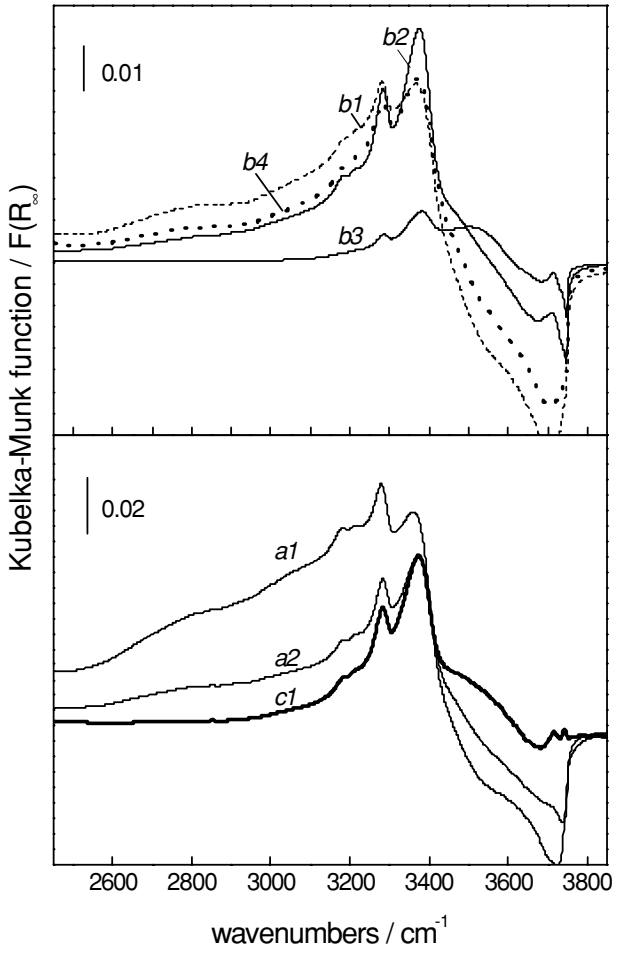

FIG. 6. DRIFT spectra of the ammonia adsorbed on the calcined aerogels, after *in situ* pretreatment in air at 300°C. Top: Spectra of the aerogels containing crystalline Mn_3O_4. Bottom: Spectra of the amorphous aerogels. Note that spectra represent difference spectra, derived as described in Section 2.

may arise around 3000 cm^{-1}. The broad vibration around 2800 cm^{-1} is likely associated with the overtone of δ_{as}(NH) (52, 53). The presence of stretching vibrations due to ammonium ions in the 3400- to 3200-cm^{-1} region, where also Lewis-bound ammonia appears, cannot be fully excluded, as some narrow bands above 3300 cm^{-1} were assigned to the unperturbed N–H groups of adsorbed NH_4^+ on H–ZSM-5, in agreement with *ab initio* calculations (54–56). However, the ν(NH) extinction coefficient of the free N–H is expected to be lower than that of hydrogen bonded N–H (54, 57). Therefore the intense vibrations observed in our study in the 3400- to 3250-cm^{-1} region are assigned to Lewis-bound ammonia. As also reported by Zecchina *et al.* (54), the intensity of the consumed OH stretching vibrations (negative bands) was correlated with the intensity of the Brønsted bands. Aerogels *a1*, *b1*, and *b4* showed the highest decrease in hydroxyls as well as the highest amount of Brønsted-bound ammonia.

The ratio N_{300}/N_{50} of the amount of ammonia adsorbed at 50°C (N_{50}) and 300°C (N_{300}), derived from the integrated ν(N–H) band areas, was taken as a measure of the mean acidity of the catalysts. The values, listed in Table 4, varied from 2.0 to 5.7%. Among the amorphous aerogels, *a1* was the aerogel with the higher ratio. Sample *b2* with crystalline Mn_3O_4, which showed very intense vibrations due to Lewis-bound ammonia at 50°C, exhibited a value, 5.7%.

3.4. Selective Catalytic Oxidation (SCO) of Ammonia

The performance of the calcined aerogels in the SCO of ammonia measured in the range 180–480°C is summarized in Table 5. Figure 7 shows the Arrhenius plots derived from the differential catalytic measurements. Activity of the amorphous aerogels was generally lower than that of the aerogels with crystalline hausmannite (bottom and top in Fig. 7, respectively). The selectivity also varied among the aerogels (Table 5). The amorphous aerogels synthesized from manganese nitrate without base addition (*a1*, *a2*) afforded a selectivity to nitrogen of 78% at 360°C. Besides nitrogen, nitrous and nitric oxide were formed. The TOF values at 300°C amounted to 0.36–0.42 $(ks)^{-1}$. The

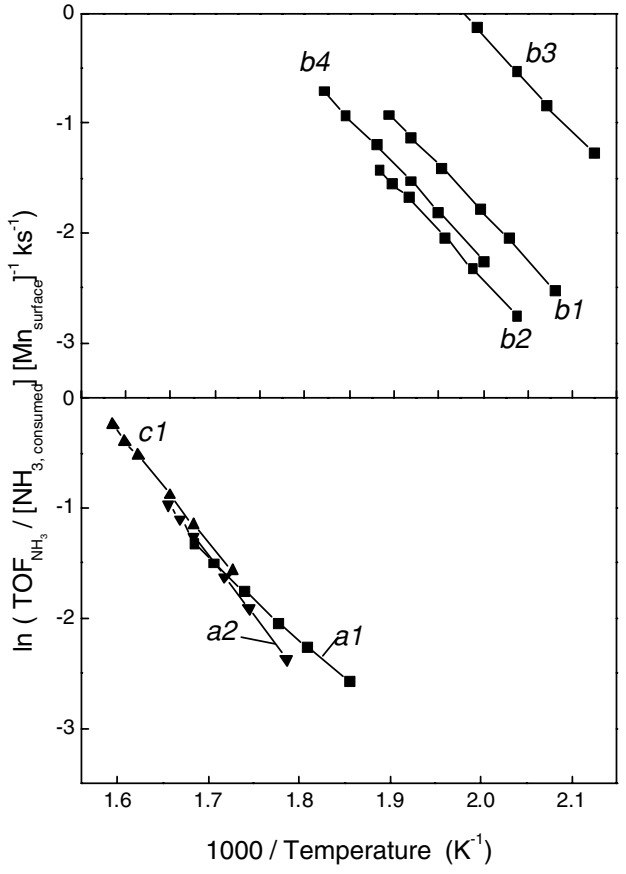

FIG. 7. Arrhenius plot of NH_3 conversion in the SCO of ammonia over manganese oxide–silica aerogels prepared under different sol–gel conditions. Bottom: Amorphous samples. Top: Aerogels containing crystalline Mn_3O_4. TOFs were computed from the converted ammonia-per-surface-manganese content (see text).

TABLE 5

Catalytic Performance of MnO_x–SiO_2 Aerogels in the Selective Catalytic Oxidation of Ammonia to N_2

Catalyst	E_{act} NH_3 (kJ mol^{-1})	E_{act} N_2 (kJ mol^{-1})	E_{act} N_2O (kJ mol^{-1})	E_{act} NO (kJ mol^{-1})	TOF[a] (ks^{-1})	rate ($\times 10^9$) (mol of NH_3 m^{-2} s^{-1})	$S(N_2)$[d] (%)	$S(N_2O)$[d] (%)
a1	72	63	—	150	0.42[b]	20.7[b]	78	13
a2	91	88	—	140	0.36[b]	5.0[b]	78	21
b1	79	71	93	—	0.56[c]	6.9[c]	23	72
b2	78	71	102	—	0.28[c]	3.7[c]	36	60
b3	81	72	97	—	2.63[c]	11.1[c]	22	74
b4	81	72	93	—	0.25[c]	4.0[c]	30	69
c1	90	84	100	135	0.81[b]	5.2[b]	66	24

[a] TOF, $NH_3/[(Mn_{surf}) \cdot ks]$, with Mn_{surf} determined by XPS and AAS.
[b] 300°C.
[c] 230°C.
[d] 360°C.

sample derived from $Mn(acac)_3$ showed higher activity ($0.81\ (ks)^{-1}$) at 300°C but combined with lower selectivity to nitrogen (66%). More nitrous oxide was formed, whereas nitric oxide was absent below 360°C. The aerogels with crystalline Mn_3O_4 (some also containing amorphous Mn_5O_8) were the most active catalysts. For sample *b3* a TOF of $2.63\ (ks)^{-1}$ was reached at 230°C, which was the highest activity among all aerogels. The main product with these catalysts was nitrous oxide, with a selectivity between 60 and 74% at 360°C, whereas selectivity to nitrogen was low (22–36%). Figure 8 shows ammonia conversion and selectivity achieved with aerogels *a1*, *c1*, and *b3*. All catalysts showed a decrease in nitrogen production with increasing temperatures, while NO production increased above 360°C; this was most pronounced with aerogels containing crystalline hausmannite.

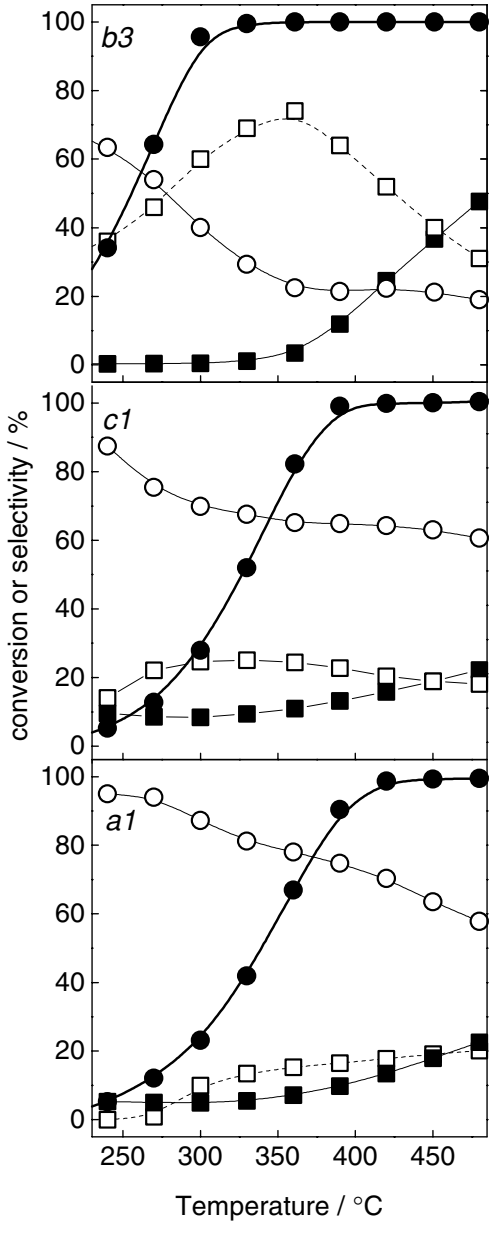

FIG. 8. Conversion of ammonia (●) and selectivity to nitrogen (○), nitrous oxide (□), and nitric oxide (■) for aerogels *a1*, *c1*, and *b3*. Integral reactor studies of SCO of ammonia in the temperature range 200–480°C.

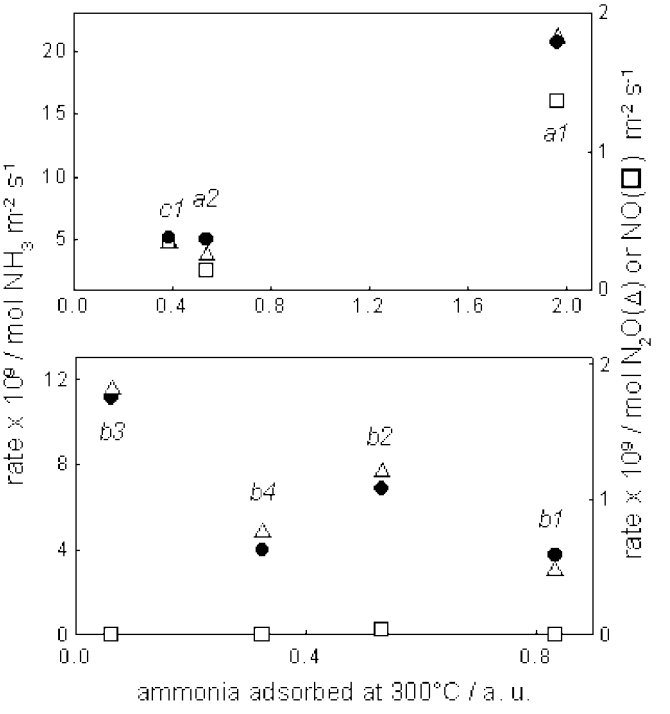

FIG. 9. Catalytic behavior of aerogels in the SCO of ammonia: rate of ammonia consumption (●) and nitric (□) and nitrous oxide (△) formation per surface area are shown as a function of the ammonia adsorption at 300°C. Top: Catalysts with high N_2 selectivity. Bottom: Catalysts with low selectivity to nitrogen. (Note that the rate of nitrogen production showed the same tendencies as ammonia consumption for all catalysts.)

Figure 9 depicts the rates of ammonia conversion and NO and N_2O production as a function of the ammonia adsorbed at 300°C, i.e., the strongly bound ammonia. Nitrogen production showed the same tendencies as the ammonia consumption for all catalysts and was therefore omitted. For the amorphous catalysts with high-to-medium selectivity to N_2 (*a1*, *a2*, *c1*), activity in SCO was correlated with the amount of ammonia adsorbed at 300°C, which consisted mainly of Lewis-bound ammonia. The rates of N_2, NO, and N_2O production were all correlated to the acidity in the same manner. Activation energies for these samples were in the range 72–91 kJ mol^{-1} for ammonia conversion. Nitrogen production showed activation energies between 63 and 88 kJ mol^{-1}, whereas NO production had an activation energy of about 140 kJ mol^{-1} (Table 5). Samples containing crystalline hausmannite (some of them also containing amorphous Mn_5O_8) showed an inverse relation between activity in SCO and ammonia adsorption (Fig. 9, bottom). Mainly N_2O was produced and NO formation started at 360°C. Activation energies were about 80 kJ mol^{-1} for

ammonia conversion, 70 kJ mol^{-1} for N_2 production, and 93–102 kJ mol^{-1} for N_2O production.

4. DISCUSSION

4.1. Structural Properties

Based on their structural and catalytic properties the manganese oxide–silica aerogels can be divided into two distinct groups, the amorphous aerogels from manganese(II) nitrate and manganese(III) triacetylacetonate, and aerogels with crystalline manganese oxide, which were also prepared from manganese(II) nitrate, but their gelation was forced by addition of a base.

Aerogels prepared from manganese nitrate and by basic gelation. The aerogels synthesized from manganese nitrate show a prominent influence of basic gelation on the morphology and state of the manganese. The forced basic gelation applied in *b1*, *b2*, *b3*, and *b4* leads to high-surface-area, mesoporous aerogels with narrow pore size distribution (Fig. 1). Indeed, high water content and basic condition enhance the dissolution rate of the polymerized silica. Below pH 8 also the condensation rate was reported to increase for aqueous solutions of silicic acid. Phenomena such as Ostwald ripening and coarsening led to stiffening of the gel and a decrease in size of micropores (47). After calcination in air at 600°C manganese oxide crystallites exist in all samples, as shown by XRD (Fig. 2) and Raman spectroscopy (Fig. 3). Segregation of the oxides is probably induced by base addition and hence the calcined aerogels show lower ammonia adsorption capacity (Table 4) and Brønsted acidity (Fig. 8). Furthermore, the surface Mn content is lower than for the amorphous samples (Table 3), although the bulk manganese content is enhanced by the strong basic conditions (*b1*, *b3*). Possibly the observed manganese oxide crystallites are "encapsulated" by amorphous silica.

Different crystalline manganese oxide phases were observed for sample *b3* by XRD and Raman spectroscopy. In line with the observation made for high-surface-area hausmannite (48), the small Mn_3O_4 crystallites were partially oxidized to X-ray amorphous Mn_5O_8 during calcination in air. Pronounced segregation was probably induced by the increased base and water content compared to the other gels, leading also to high surface area and mesoporosity (47). Analogously, for aerogel *b4* prepared with twice the amount of aqueous ammonia compared to *b1*, slightly larger hausmannite crystallites were identified by XRD (Fig. 2). Based on the reduction profile the presence of a significant amount of Mn_5O_8 on this aerogel can be excluded (Fig. 4). The higher temperature needed for reduction of the manganese is probably related to the larger crystallites, as the reference oxide hausmannite is reduced at higher temperatures. Concomitantly, the ammonia adsorption capacity (Table 4) of *b4* is slightly lower compared to that of *b1*. On both samples probably dispersed manganese oxide species coexist, as indicated by the pronounced number of acid hydroxyl groups in DRIFTS (Fig. 5). Commercial hausmannite, under ambient conditions, showed small signals of Lewis- and traces of Brønsted-bound ammonia.

Amorphous aerogels prepared from manganese(II) nitrate or manganese(III) acetylacetonate. The amorphous aerogels prepared from manganese nitrate without base addition show only highly dispersed manganese oxide species in Raman spectroscopy (Fig. 3). Predominance of dispersed manganese oxide emerges also from DRIFT spectroscopy (Fig. 5), where acid hydroxyls are detected in large amounts, and correspondingly high Brønsted acidity is observed (Fig. 6). The aerogels are micro- and mesoporous, which may be due to the absence of base during preparation.

The aerogel prepared by manganese triacetlyacetonate shows low propensity for formation of manganese oxide aggregates with forced basic gelation, affording good dispersion of the manganese together with high surface manganese content. Segregation of the components is suppressed to a large extent for the aerogels made by $Mn(acac)_3$, due to the lower reactivity of the complex. Manganese oxide nanoparticles are present after calcination, as seen by Raman spectroscopy. Surface acidity is in general lower than that of the amorphous aerogels prepared from manganese nitrate, due to the lower dispersion of the manganese. Concomitantly *c1* shows low ammonia adsorption and no Brønsted acidity (Fig. 6). In the TPR profile (Fig. 4) pronounced broadening of the signal is probably due to the presence of manganese oxide nanoparticles, as indicated by Raman spectroscopy, whereas the symmetric signal at 350–360°C may be related to the dispersed manganese oxide species, similar to that found for the amorphous aerogels prepared by manganese nitrate. The precursor has only little influence on the textural properties of the calcined aerogels, as similar surface area and pore volumes are found for *c1* and *b4*.

Effect of prehydrolysis. Prehydrolysis of the silica did not enhance dispersion of the manganese in the case of the manganese(II) nitrate precursor (*a2*). Interaction of Mn(II) with the silica is probably weak, as also indicated by the loss of manganese during extraction with supercritical CO_2, leading to low bulk manganese content for some aerogels (1–20% lower than the nominal value).

4.2. Catalytic Properties

The state of the manganese could be identified as the most crucial factor determining the catalytic properties in the SCO of ammonia. The main difference in catalytic behavior is observed between the aerogels with crystalline manganese oxide and the amorphous aerogels. The catalysts containing substantial amounts of manganese oxide exhibit higher activity and remarkable selectivity to N_2O

(60–74%), whereas the amorphous aerogels afford a selectivity to nitrogen up to 78%. High selectivity toward nitrous oxide was observed also for hausmannite above 150°C, and nitric oxide formation started at 250°C (58). Among the aerogels investigated the activity per surface manganese content and the rate per surface area are highest for *b3*. Activity toward nitrous oxide production correlates with the presence of the manganese oxide species reducible at temperatures below 220°C (Fig. 4). This may be due to the presence of Mn_5O_8 (TPR, Raman), whose oxidation state is higher than that of Mn_3O_4. Mn_2O_3 and MnO_2 were more active per surface area in SCO than Mn_3O_4 (58). Additionally to the Mn^{4+} content, the metastability of this oxide may play an important role in its activity in N_2O formation.

Differential reactor measurements for these catalysts in the range 200–280°C revealed that the activation energy for N_2O formation is higher than that for nitrogen, which explains the appearance of the former at higher temperatures. Also for Mn_2O_3, producing mainly N_2O, an activation energy very close to these samples was determined (28). The conversion of ammonia shows a negative correlation to the amount of strongly bound ammonia at 300°C; concomitantly selectivity to nitrous oxide decreases (Fig. 9, bottom). Note that on *b4* no Mn_5O_8 is detected (TPR), showing therefore lower activity.

In contrast to the samples with manganese oxide crystallites, increasing ammonia adsorption enhances the ammonia conversion for the highly dispersed manganese oxide–silica aerogels (Fig. 9, top). Concomitantly, the relative acidity of the aerogels increases, as revealed by the share of ammonia adsorbed at 300°C (Table 4). The samples, for which the presence of manganese oxide clusters is not revealed in Raman spectroscopy, are the most selective to nitrogen. The large amount of dispersed manganese oxide is probably the reason for the high amount of Lewis-bound ammonia at 300°C. The acidity and hence the adsorption strength of the ammonia may play an important role in the dehydrogenation step of ammonia.

5. CONCLUSIONS

Manganese oxide–silica mixed oxide aerogels were synthesized by the sol–gel method combined with supercritical drying. Depending on the sol–gel conditions (precursor, hydrolysis, and gelation conditions) and the calcination temperature, the structural, chemical, and catalytic properties of the aerogels changed drastically.

Textural properties of the aerogels were strongly influenced by base addition during gelation and by the calcination temperature. Reactivity of the manganese precursor, base content of the sol, and calcination temperature affected the state of the manganese. Depending on conditions different manganese oxide species formed, ranging from crystalline Mn_3O_4 and amorphous Mn_5O_8 to highly dispersed manganese oxide. Crystalline Mn_3O_4 and amorphous Mn_5O_8 were observed when using Mn(II) nitrate and base, whereas with Mn(III) $(acac)_3$ the formation of amorphous manganese nanoparticles was favored under the same conditions. Highly dispersed amorphous mixed oxides could be prepared using Mn(II) nitrate without base.

The catalytic properties of the aerogels were tested using the selective catalytic oxidation of ammonia. The amorphous aerogels with highly dispersed manganese oxide showed high selectivity to nitrogen (78%), whereas the aerogels containing crystalline Mn_3O_4 and amorphous Mn_5O_8 afforded N_2O as the main product, reaching a selectivity of 74% at 360°C. The propensity of the aerogels to form nitrogen was found to be correlated with the abundance of Lewis-bound ammonia, which was higher on the amorphous dispersed mixed oxides.

ACKNOWLEDGMENTS

The authors thank Dr. Jan-Dierk Grunwaldt for XPS measurements, and Dr. M. Maciejewski for XRD measurements.

REFERENCES

1. Pajonk, G. M., *Appl. Catal.* **72**, 217 (1991).
2. Ward, D. A., and Ko, E. I., *Ind. Eng. Chem. Res.* **34**, 421 (1995).
3. Schneider, M., and Baiker, A., *Catal. Rev.–Sci. Eng.* **37**, 515 (1995).
4. Craciun, R., *Catal. Lett.* **55**, 25 (1998).
5. Kou, Y., Zhang, B., Niu, J. Z., Li, S. B., Wang, H. L., Tanaka, T., and Yoshida, S., *J. Catal.* **173**, 399 (1998).
6. Koh, D. J., Chung, J. S., Kim, Y. G., Lee, J. S., Nam, I. S., and Moon, S. H., *J. Catal.* **138**, 630 (1992).
7. Machida, M., Eguchi, K., and Arai, H., *J. Catal.* **123**, 477 (1990).
8. Machida, M., Sato, A., Kijima, T., Inoue, H., Eguchi, K., and Arai, H., *Catal. Today* **26**, 239 (1995).
9. Aylor, A. W., Lobree, L. J., Reimer, J. A., and Bell, A. T., *J. Catal.* **170**, 390 (1997).
10. Campa, M. C., Pietrogiacomi, D., Tuti, S., Ferraris, G., and Indovina, V., *Appl. Catal. B* **18**, 151 (1998).
11. Kijlstra, W. S., Brands, D. S., Poels, E. K., and Bliek, A., *J. Catal.* **171**, 219 (1997).
12. Kapteijn, F., van Langeveld, A. D., Moulijn, J. A., Andreini, A., Ramis, G., and Busca, G., *J. Catal.* **150**, 105 (1994).
13. Grzybek, T., Pasel, J., and Papp, H., *Phys. Chem. Chem. Phys.* **1**, 341 (1999).
14. Ma, J., Chuah, G. K., Jaenicke, S., Gopalakrishnan, R., and Tan, K. L., *Ber. Bunsen-Ges. Phys. Chem.* **99**, 184 (1995).
15. Ma, J., Chuah, G. K., Jaenicke, S., Gopalakrishnan, R., and Tan, K. L., *Ber. Bunsen-Ges. Phys. Chem.* **100**, 585 (1996).
16. Ammundsen, B., Jones, D. J., Roziere, J., and Burns, G. R., *Chem. Mater.* **9**, 3236 (1997).
17. Ammundsen, B., Burns, G. R., Amran, A., and Friberg, E., *J. Sol.-Gel Sci. Technol.* **2**, 341 (1994).
18. Ammundsen, B., Burns, G. R., Jones, D. J., and Roziere, J., *J. Sol.-Gel. Sci. Technol.* **8**, 331 (1997).
19. Kurihara, L. K., and Suib, S. L., *Chem. Mater.* **5**, 609 (1993).
20. Taguchi, H., Ohota, A., and Nagao, M., *J. Mater. Sci.* **31**, 5697 (1996).
21. Oyoung, C. L., and Suib, S. L., *Stud. Surf. Sci. Catal.* **105**, 189 (1997).
22. Brock, S. L., Duan, N. G., Tian, Z. R., Giraldo, O., Zhou, H., and Suib, S. L., *Chem. Mater.* **10**, 2619 (1998).

23. Ching, S., and Suib, S., *Comments Inorg. Chem.* **19/5**, 263 (1997).
24. LeGoff, P., Baffier, N., Bach, S., and Pereira-Ramos, J. P., *J. Mater. Chem.* **4/1**, 133 (1994).
25. Passerini, S., Coustier, F., Giorgetti, M., and Smyrl, W. H., *Electrochem. Solid State Lett.* **2**, 483 (1999).
26. Yan, L. C., and Thompson, L. T., *Appl. Catal. A* **171**, 219 (1998).
27. Il'chenko, N. I., and Golodets, G. I., *J. Catal.* **39**, 57 (1975).
28. Germain, J. E., and Perez, R., *Bull. Soc. Chim. Fr.* **5**, 2042 (1972).
29. Wöllner, A., Lange, F., Schmelz, H., and Knözinger, H., *Appl. Catal. A* **94**, 181 (1993).
30. Amblard, M., Burch, R., and Southward, B. W. L., *Appl. Catal. B* **22**, L159 (1999).
31. Amores, J. M. G., Escribano, V. S., Ramis, G., and Busca, G., *Appl. Catal. B* **13**, 45 (1997).
32. Yahiro, H., Nakai, T., Shiotani, M., and Yamanaka, S., *J. Catal.* **187**, 249 (1999).
33. Wu, Y., Yu, T., Bo-sheng, D., Wang, C., Xie, X., Yu, Z., Fan, S., Fan, Z., and Wang, L., *J. Catal.* **120**, 88 (1989).
34. Lietti, L., Ramella, C., Groppi, G., and Forzatti, P., *Appl. Catal. B* **21**, 89 (1999).
35. Long, R. Q., and Yang, R. T., *Chem. Commun.* 1651 (2000).
36. Meyer, R. J., Pietsch, E. H. E., and Becke-Goehring, M., Eds., "Gmelin Handbook of Inorganic and Organometallic Chemistry," Vol. Mn[C1]. Springer, Berlin, 1975.
37. "CRC Handbook of Chemistry and Physics." (D. R. Lide, Ed.) CRC Press, London, 1993.
38. Monti, D. M., and Baiker, A., *J. Catal.* **83**, 323 (1983).
39. Wagner, C. D., Davis, L. E., Zeller, M. V., Taylor, J. A., Raymond, R. M., and Gale, L. H., *Surf. Interface Anal.* **3**, 211 (1981).
40. Vansant, E. F., Van Der Voort, P., and Vrancken, K. C., *Stud. Surf. Sci. Catal.* **93**, 59 (1995).
41. Klug, H. P., and Alexander, L. E., "X-Ray Diffraction Procedures for Polycrystalline and Amorphous Materials." Wiley, New York, 1974.
42. Feitknecht, W., and Schindler, P., *Pure Appl.Chem.* **6**, 167 (1963).
43. Weitz, E., and Kampf, M., *Z. Angew. Chem.* **37**, 391 (1924).
44. Stobbe, E. R., de Boer, B. A., and Geus, J. W., *Catal. Today* **47**, 161 (1999).
45. Strohmeier, B. R., and Hercules, D. M., *J. Phys. Chem.* **88**, 4922 (1984).
46. Kapteijn, F., van Langeveld, A. D., Moulijn, J. A., Andreini, A., Vuurman, M. A., Turek, A. M., Jehng, J. M., and Wachs, I. E., *J. Catal.* **150**, 94 (1994).
47. Brinker, C. J., and Scherer, G. W., "Sol–Gel Science, the Physics and Chemistry of Sol–Gel Processing." Academic Press, San Diego, 1990.
48. Fritsch, S., Sarrias, J., Rousset, A., and Kulkarni, G. U., *Mater. Res. Bull.* **33**, 1185 (1998).
49. Briggs, D., and Seah, M. P., *in* "Practical Surface Analysis," p. 494. Wiley, New York, 1982.
50. Fabrizioli, P., Burgener, M., Bürgi, T., van Doorslaer, S., and Baiker, A., *J. Mater. Chem.*, in press.
51. Pittman, R. M., and Bell, A. T., *Catal. Lett.* **24**, 1 (1994).
52. Nakamoto, K., *in* "Infrared and Raman Spectra of Inorganic and Coordination Compounds," Part A, p. 192. Wiley, New York, 1995.
53. Vedder, W., and Hornig, D. F., *J. Chem. Phys.* **35**(5), 1560 (1961).
54. Zecchina, A., Marchese, L., Bordiga, S., Pazè, C., and Gianotti, E., *J. Phys. Chem. B* **101**, 10128 (1997).
55. Eng, J., and Bartholomew, H., *J. Catal.* **171**, 27 (1997).
56. Teunissen, E. H., van Santen, R. A., Jansen, A. P. J., and van Duijneveldt, F. B., *J. Phys. Chem.* **97**, 203 (1993).
57. Pimentel, G. C., and McClellan, A. L., *in* "The Hydrogen Bond" (L. Pauling, Ed.), p. 221. Freeman, San Francisco, 1960.
58. Kapteijn, F., Singoredjo, L., Andreini, A., and Moulijn, J., *Appl. Catal. B* **3**, 173 (1994).